A Fast 2.5-D Parallel Multilevel Fast Multipole Algorithm Solver

***Jan Fostier*[1] *and Femke Olyslager*[1]**
[1]Department of Information Technology (INTEC), Ghent University,
Sint-Pietersnieuwstraat 41, B-9000 Ghent, Belgium.
e-mail: jan.fostier@intec.ugent.be; femke.olyslager@intec.ugent.be

Abstract

We present a 2.5-D Multilevel Fast Multipole Algorithm (MLFMA) that is capable of solving large and complex environments consisting of multiple dielectric and conducting objects. The solver is augmented by means of an asynchronous parallelization. Its accuracy is demonstrated by comparing the analytical and numerical radar cross section (RCS) of a canonical example with a size of 15 000 wavelengths. An open-source reference implementation of the software is presented to the community free of charge.

1. Introduction

This paper is concerned with the development of an efficient 2.5-D MLFMA solver that is capable of handling both dielectric and PEC objects. The term '2.5-D' denotes the ability to handle 3D sources in a 2D environment. The boundary integral equation that was employed and its classic Method of Moment (MoM) solution were first developed in [1] to study the behavior of waveguides in layered media. In a later effort, the Impedance Matrix Localization (IML) method was used to sparsify the system matrix [2]. This allowed for the application the integral equation in casu to the prediction of indoor wave propagation. Other applications of 2.5-D simulations can be found in research topics such as imaging and tomography.

Recently, we have proposed a kernel-independent asynchronous parallel MLFMA applied to 2D transversal magnetic (TM) scattering problems [3]. The asynchronous algorithm allows for an efficient parallelization of simulations that involve multiple dielectric objects and/or PEC objects and is well suited for lower-cost parallel architectures. In this contribution, we report the application of this asynchronous parallel framework to the 2.5-D integral equation. The extension from 2D to 2.5-D leads to a significant increase in complexity because of the coupling between TM and TE, hence doubling the number of unknowns. Compared to 3D simulations, 2D and 2.5-D solvers allow for significantly larger simulations in terms of wavelengths, however, the interactions between the discretized elements have a longer action range due to the slower decay of the Green function. As was the case for the 2D solver, the implementation of the algorithm is open source and can be downloaded free of charge [4].

2. Method of Moments (MoM)

Consider a number of 2D homogeneous dielectric and PEC cylindrical objects of arbitrary shape that are embedded in a background medium or in another dielectric. The objects do not touch or overlap. The objects are illuminated by an incoming electromagnetic field $\mathbf{E}^{\text{inc}}, \mathbf{H}^{\text{inc}}$. If the total number of dielectric objects is D, then the number of homogeneous regions is $D+1$. Using the inverse spatial Fourier transform in the z-direction (the longitudinal direction), the incoming and scattered fields can be assembled from their respective spectra, e.g. for the electric field

$$\mathbf{E}(\mathbf{r}) = \frac{1}{2\pi} \int_{-\infty}^{+\infty} \mathbf{E}(\boldsymbol{\rho}, \beta) e^{-j\beta z} \mathrm{d}\beta, \tag{1}$$

with $\boldsymbol{\rho} = x\mathbf{u}_x + y\mathbf{u}_y$. Only the β components ranged in $[-k_i, k_i]$ (with $k_i = \omega\sqrt{\epsilon_i \mu_i}$) contribute to the propagating fields in medium i. In what follows, we focus on a single β component and suppress the time and z-dependence $e^{j(\omega t - \beta z)}$ without introducing new notations for the field components.

From elementary electromagnetic theory, it is found that the longitudinal field components E_z and H_z satisfy the Helmholtz equation in each homogeneous medium i.

$$\frac{\partial^2 \mathrm{F}_z}{\partial x^2} + \frac{\partial^2 \mathrm{F}_z}{\partial y^2} + \gamma_i^2 \mathrm{F}_z = 0, \tag{2}$$

with $\gamma_i^2 = k_i^2 - \beta^2$ and $\mathrm{F} = \mathrm{E}$ or $\mathrm{F} = \mathrm{H}$. In the local tangential coordinate system to boundary curve C_i of medium i, the E_t and H_t components can be expressed from the longitudinal components as follows

$$\begin{aligned}
\mathrm{E}_t &= -\frac{j\beta}{\gamma_i^2}\frac{\partial \mathrm{E}_z}{\partial t} + \frac{j\omega\mu_i}{\gamma_i^2}\frac{\partial \mathrm{H}_z}{\partial n}, \\
\mathrm{H}_t &= -\frac{j\beta}{\gamma_i^2}\frac{\partial \mathrm{H}_z}{\partial t} - \frac{j\omega\epsilon_i}{\gamma_i^2}\frac{\partial \mathrm{E}_z}{\partial n}.
\end{aligned} \tag{3}$$

By making use of Green's identity and by eliminating the normal derivatives using (3), the fields in a point $\boldsymbol{\rho}$ within medium i can be expressed as a contour integral along its boundary C_i (see [1]):

$$\mathrm{E}_z(\boldsymbol{\rho}) = \oint_{C_i} \mathrm{d}c' \left[\mathrm{E}_z(\boldsymbol{\rho'}) \frac{\partial G_i(\boldsymbol{\rho}|\boldsymbol{\rho'})}{\partial n'} - \left(\frac{j\gamma_i^2}{\omega\epsilon_i} \mathrm{H}_t(\boldsymbol{\rho'}) - \frac{\beta}{\omega\epsilon_i} \frac{\partial \mathrm{H}_z(\boldsymbol{\rho'})}{\partial t'} \right) G_i(\boldsymbol{\rho}|\boldsymbol{\rho'}) \right], \tag{4}$$

$$\begin{aligned}
\mathrm{E}_t(\boldsymbol{\rho}) &= \oint_{C_i} \mathrm{d}c' \left[\frac{j\omega\mu_i}{\gamma_j^2} \mathrm{H}_z(\boldsymbol{\rho'}) \frac{\partial^2 G_i(\boldsymbol{\rho}|\boldsymbol{\rho'})}{\partial n \partial n'} + \frac{j\omega\mu_i}{\gamma_i^2} \left(\frac{j\gamma_i^2}{\omega\mu_i} \mathrm{E}_t(\boldsymbol{\rho'}) - \frac{\beta}{\omega\mu_i} \frac{\partial \mathrm{E}_z(\boldsymbol{\rho'})}{\partial t'} \right) \frac{\partial G_i(\boldsymbol{\rho}|\boldsymbol{\rho'})}{\partial n} \right] \\
&+ \oint_{C_i} \mathrm{d}c' \left[-\frac{j\beta}{\gamma_i^2} \mathrm{E}_z(\boldsymbol{\rho'}) \frac{\partial^2 G_i(\boldsymbol{\rho}|\boldsymbol{\rho'})}{\partial t \partial n'} + \frac{j\beta}{\gamma_i^2} \left(\frac{j\gamma_i^2}{\omega\epsilon_i} \mathrm{H}_t(\boldsymbol{\rho'}) - \frac{\beta}{\omega\epsilon_i} \frac{\partial \mathrm{H}_z(\boldsymbol{\rho'})}{\partial t'} \right) \frac{\partial G_i(\boldsymbol{\rho}|\boldsymbol{\rho'})}{\partial t} \right].
\end{aligned} \tag{5}$$

The expression for $\mathrm{H}_z(\boldsymbol{\rho})$ and $\mathrm{H}_t(\boldsymbol{\rho})$ can be obtained from (4) and (5) respectively, by using the duality principle ($\mathrm{E} \rightarrow \mathrm{H}$, $\mathrm{H} \rightarrow -\mathrm{E}$, $\epsilon_i \leftrightarrow \mu_i$). The two dimensional Green function is given by

$$G_i(\boldsymbol{\rho}|\boldsymbol{\rho'}) = \frac{j}{4} H_0^{(2)}(\gamma_i|\boldsymbol{\rho} - \boldsymbol{\rho'}|). \tag{6}$$

The final set of integral equations is obtained by expressing the continuity of the field components E_z, H_z, E_t, H_t across dielectric boundaries. For a PEC body, only the H_z and H_t unknowns remain and the corresponding integral equation is obtained by expressing that the tangential electrical fields vanish at its boundary. In the appropriate media, a contribution from an excitation source needs to be taken into account (this is usually the background medium).

The contour is divided into a number of line segments with a length of $\lambda/10$. For the longitudinal components E_z and H_z, overlapping triangular basis functions are defined. Conversely, pulse basis functions are used to test E_z and H_z whereas E_t and H_t are tested by triangular basis functions. A consistent Galerkin MoM is obtained in this way.

3. High frequency MLFMA

In this section, the application of the MLFMA to the MoM is discussed. In this approach, we consider problems that are extremely large compared to the wavelength, motivating a high-frequency MLFMA based on plane wave expansion. For a good introduction to the mathematics and data structures of the MLFMA, we refer to [5].

The geometry is enclosed in a square rectangle which is hierarchically subdivided into four quadrants. This process is stopped when the lowest level box size is approximately $0.15 - 0.5\lambda$. In this way, a tree of boxes is obtained. Two boxes at a certain level of the tree interact with each other when they are sufficiently separated from each other while their respective parent boxes are not. This interaction is mathematically expressed through the following factorization of the Green function:

$$\frac{j}{4} H_0^{(2)}(\gamma|\boldsymbol{\rho}_o - \boldsymbol{\rho}_s|) \approx \frac{j}{4} \sum_{n=-Q}^{n=+Q} [e^{j\boldsymbol{\gamma}_n \cdot (\boldsymbol{\rho}_s - \mathbf{P}_s)} T_n(\mathbf{P}_o - \mathbf{P}_s) e^{-j\boldsymbol{\gamma}_n \cdot (\boldsymbol{\rho}_0 - \mathbf{P}_o)}] \tag{7}$$

where $\mathbf{P}_s$ and $\mathbf{P}_o$ are, respectively, the centers of the source and the observation group and where $\boldsymbol{\rho}_s$ and $\boldsymbol{\rho}_o$ are two arbitrary points on the segments in the source and observation groups respectively. $\boldsymbol{\gamma}_n$ are wavevectors along equidistant directions ϕ_n, $n = -Q, ..., 0, ..., Q$ and T_n is the translation operator given by

$$T_n(\mathbf{P}) = \frac{1}{2Q+1} \sum_{n'=-Q}^{n'=+Q} H_{n'}^{(2)}(\gamma|\mathbf{P}|) e^{jn'(\Phi-\phi_n-\frac{\pi}{2})} \tag{8}$$

with Φ the angle between $\mathbf{P}$ and the x-axis.

The first part (the aggregation) in (7) depends only on the segments in the source group and is an expansion of plane waves along directions ϕ_n. The second part depends only on the centers of the observation and the source group and represents the translation of plane waves. The third part (the disaggregation) depends only on the segments of the observation group and is an aggregation of incoming plane waves.

In the MLFMA this is extrapolated hierarchically by assembling groups into groups and so on. In that way all the interactions, normally requiring a computational complexity of $O(N^2)$, can be reduced to $O(N \log N)$.

At first glance it would appear that four radiation patterns – one for each field component – are necessary to perform the far interactions. However, only the radiation patterns containing the far field of the E_z and H_z components are required. Equations (3) can be used to obtain the other two components E_t and H_t. This observation results in a reduction by a factor of two in the memory requirements for storing the outgoing and incoming far field patterns and eliminates obsolete shifting, interpolation and translation operations.

3.1 Asynchronous parallelization

Traditional implementations of the parallel MLFMA are essentially synchronous. They are characterized by alternating phases of calculations and communications. By using complex load-balancing schemes, very large simulations at good efficiencies have been demonstrated for large 3D PEC objects by several research groups. This synchronous approach, however, works only well for single objects. When considering simulations with multiple homogeneous regions of different sizes, the partitioning of the domain across the participating nodes will result in a situation where larger MLFMA trees are distributed among many nodes while smaller trees are located on just a few nodes, or possibly even on a single one. It is clear that a serial processing of these trees will result in a poor efficiency.

The asynchronous framework allows the nodes to perform calculations for any tree in a flexible way, i.e. a node can switch from working on one tree to another and minimize the time it spends idling. The workload is divided in small packets, involving the calculation of near interactions, aggregations, translations or disaggregations. The main principle is to handle first those packets that might result in data that another processor might need. If for a certain packet information from another processor is needed that is not yet available then it will be rescheduled to be handled later. As soon as data is available for another node, it will be scheduled for sending. The actual communication commences as soon as the other processor is ready to accept it. This means that communication between nodes is spread through time instead of occurring in bursts, which results in a more efficient use of the available bandwidth, making it useful for a slower, but cheaper Gigabit Ethernet network interconnect. Of course the defining and scheduling of all the work packets is a complex task. For a detailed description of the algorithm, we refer the reader to [3].

4. Example

We consider a circular dielectric cylinder (diameter $= 7\,500\lambda_0$, $\epsilon_r = 4$) concentrically embedded in a circular dielectric (diameter $= 15\,000\lambda_0$, $\epsilon_r = 2$) cylinder. The cylinders are illuminated by a transversal magnetic (TM) plane wave incident at an angle of 20° with the xy-plane ($\beta/\gamma_0 = \tan(20^\circ)$). The problem was discretized into $4\,443\,792$ unknowns. The numerical solution was obtained on a parallel system consisting of 20 processors (10 dual-core AMD Opteron 270) with two GByte of memory each. A total number of $1\,601$ iterations were required for the relative residual error to drop below $5 \cdot 10^{-3}$. A $4\lambda_0 \times 4\lambda_0$ preconditioner was used. The bistatic radar cross-section (RCS) was determined for both polarizations (VV and VH) in three million equidistant angles and compared to the analytical solutions (see Fig. 1). RMS errors of 0.12 dB and 0.38 dB were obtained for the VV and VH polarization respectively.

5. Conclusion

We have developed a 2.5-D parallel asynchronous MLFMA solver that is suitable for dielectric and PEC objects. Simulation and analytic results for a very large cylindrical object with a diameter of $15\,000\lambda$ and more than four million of unknowns were found to be in excellent agreement. The source code of the software can be downloaded free of charge.

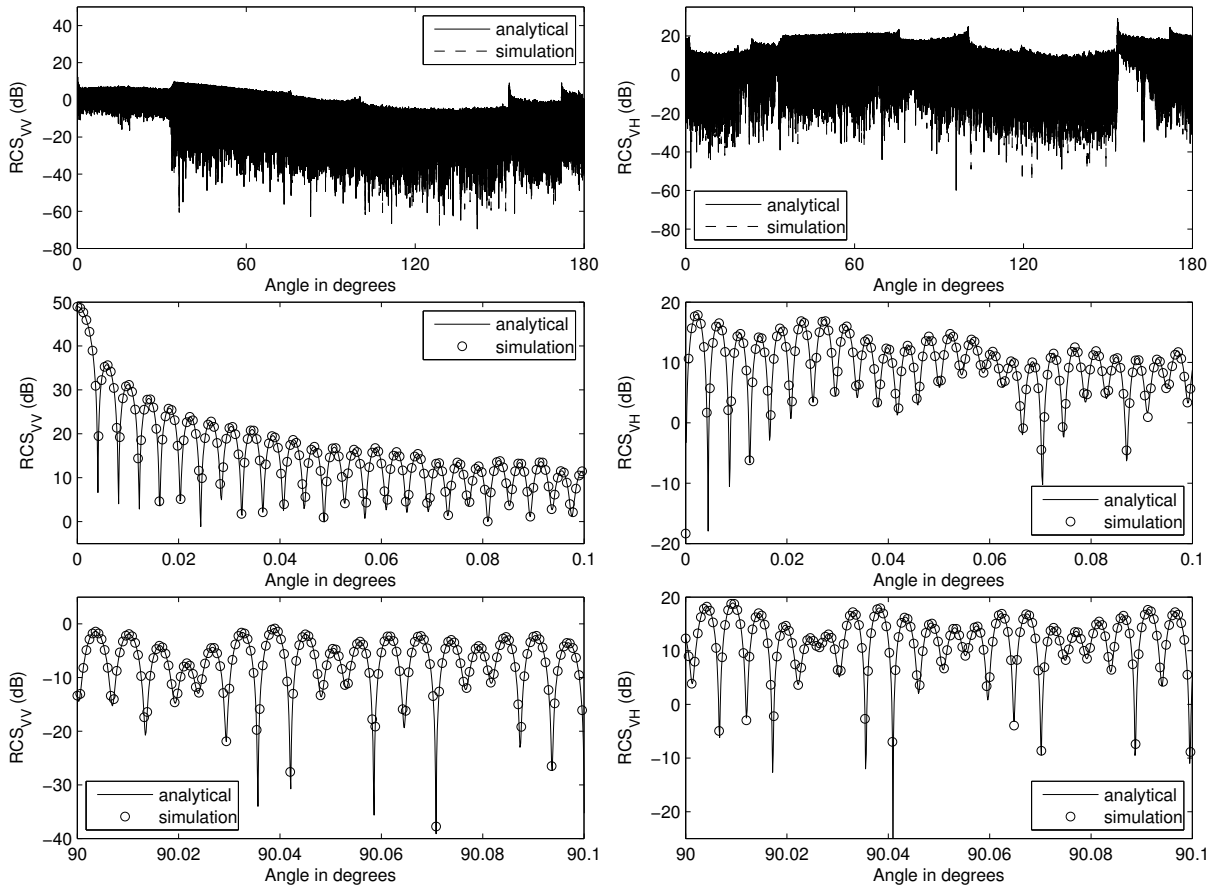

Figure 1: Comparison between the analytical and calculated bistatic RCS (left: VV polarization; right: VH polarization) of a $7\,500\ \lambda_0$ dielectric cylinder ($\epsilon_r = 4$) embedded into a $15\,000\ \lambda_0$ dielectric cylinder ($\epsilon_r = 2$) : $\theta \in [0°, 180°]$ (top), $\theta \in [0°, 0.1°]$ (middle), $\theta \in [90°, 90.1°]$ (bottom).

Acknowledgments

The work of J. Fostier was supported by a doctoral grant from the Institute for the Promotion of Innovation through Science and Technology in Flanders (IWT-Vlaanderen). The authors would like to thank Bart Dhoedt and Stijn De Smet for a generous allocation of computational resources at the Belnet GRID computing infrastructure.

References

[1] F. Olyslager, D. De Zutter, and K. Blomme, "Rigourous Analysis of the Propagation Characteristics of General Lossless and Lossy Multiconductor Transmission Lines in Multilayered Media," *IEEE Trans. Microw. Theory Tech.*, 1993, **41**(1), pp. 79–88.

[2] B. De Backer, F. Olyslager, and D. De Zutter, "An Integral Equation Approach to the Prediction of Indoor Wave Propagation," *Radio Science*, 1997, **32**(5), pp. 1833–1850.

[3] J. Fostier and F. Olyslager, "An Asynchronous Parallel MLFMA for Scattering at Multiple Dielectric Objects," *Accepted for publication in the IEEE Trans. Ant. Propag.*, 2008.

[4] J. Fostier, J. Peeters, and F. Olyslager, "Open FMM, http://openfmm.intec.ugent.be," 2008.

[5] W. C. Chew, J.-M. Jin, E. Michielssen, and J. Song, *Fast and Efficient Algorithms in Computational Electromagnetics*, Artech House, Boston, 2001.

International Union
of Radio Science

Union Radio Scientifique
Internationale

XXIX General
Assembly
7-16 August 2008
Chicago, USA

Support: If you have problems or questions related to the installation of this disc, please contact the 3WAIsmen at FAX: (818) 952-0183 or e-mail: wais3men@yahoo.com

WAIs3men